https://doi.org/10.5194/egusphere-2026-2111
Preprint. Discussion started: 22 April 2026

Quantifying temperature dependence of Fe reduction in humid tropical soils: a Bayesian model-data integration

Shibli Sadik Tulip[1], Sherlynette Pérez Castro[2], Aaron Thompson[2], Jennifer Pett-Ridge[3,4,5], and Salvatore Calabrese[1]

[1]Department of Biological and Agricultural Engineering, Texas A&M University, College Station, TX, USA
[2]Department of Crop and Soil Sciences, University of Georgia, Athens, GA, USA
[3]Lawrence Livermore National Laboratory, Physical and Life Science Directorate, Livermore, CA, USA
[4]Life and Environmental Sciences Department, University of California, Merced, CA, USA
[5]Innovative Genomics Institute, University of California, Berkeley, CA, USA

Correspondence: Salvatore Calabrese (salvatore.calabrese@ag.tamu.edu)

Abstract. Humid tropical forests are critical regulators of the global carbon (C) cycle, yet their soil C stocks are increasingly vulnerable to warming. Predicting potential losses requires a mechanistic understanding of the processes that govern soil C stabilization and mineralization, particularly in Fe-rich soils, where iron (Fe) redox cycling plays a dual role in both protecting and decomposing organic matter. However, the temperature dependency of these Fe-mediated processes remains poorly understood. In this study, we quantified the temperature dependence of Fe^{III} reduction by conducting anoxic incubations at 23, 27, and 33 °C and calibrating four kinetic models of increasing complexity to estimate the Q_{10} and Arrhenius (Ea) using a Markov Chain Monte Carlo (MCMC) framework. Model performance was evaluated using Bayesian information criteria (WAIC, LOO, and LPML) to assess fit, complexity and uncertainty. Short-term warming significantly accelerated Fe-reduction rates, potentially destabilizing mineral-associated organic carbon and enhancing microbial respiration. Estimated Q_{10} and Ea values ranged from 1.5 to 2.1 and 30.8 to 56.5 kJ mol^{-1} respectively, comparable to the temperature sensitivity values measured in temperate and tropical biomes. With the available data, Bayesian information criteria preferred the simplest one pool Fe^{II} model due to its parsimony. In contrast, the most complex (three pool) model, which includes dissolved organic carbon (DOC) dynamics alongside Fe reduction and oxidation, was generally the least preferred by Bayesian information criteria due to increased uncertainty from unconstrained additional processes. These results underscore the importance of temperature-dependent Fe redox processes in regulating soil C cycle in humid tropical soils and emphasize the need to balance model complexity with data availability when modeling coupled C-Fe interactions.

1 Introduction

In humid tropical forests, the response of soil organic carbon (SOC) to warming is complicated by its close interactions with Fe minerals (Cusack et al., 2016; Nottingham et al., 2020; Scharlemann et al., 2014; Wood et al., 2025). Humid tropical soils experience relatively stable temperatures and frequent rainfall that enhance redox cycling in soil microsites (Liptzin et al., 2011; Hall et al., 2013). Under anoxic conditions, microbial communities can use Fe reduction to obtain energy from

https://doi.org/10.5194/egusphere-2026-2111
Preprint. Discussion started: 22 April 2026

organic substrates, reducing Fe^{III} to Fe^{II} while decomposing organic matter (Lovley, 1991; Roden and Wetzel, 1996; Roden, 2004; Dubinsky et al., 2010). This process can also destabilize Fe^{III}–SOC associations, releasing previously protected SOC (Bhattacharyya et al., 2018), which in turn becomes available for microbial decomposition (Song et al., 2022; Tang et al., 2025). Conversely, Fe oxidation can re-stabilize SOC by promoting new Fe^{III} mineral formation and re-sorption of organic carbon (Thaymuang et al., 2013; Souza et al., 2018; Silva et al., 2015; Silva Neto et al., 2008). The redox-driven coupling of Fe cycling and SOC turnover thus introduces a dynamic feedback, where warming may accelerate both SOC release and re-stabilization, depending on redox conditions. While it is often assumed that tropical soils are less sensitive to temperature than cooler soils (Feeley and Silman, 2010), whether warming make these soils vulnerable to redox-driven changes in Fe-C dynamics and in turn SOC decomposition remains to be quantified (Cusack et al., 2016).

Temperature profoundly affects the soil carbon cycle by stimulating microbial activity and increasing heterotrophic respiration, which together accelerate organic matter decomposition (Davidson and Janssens, 2006; Allison et al., 2010; Wieder et al., 2013; Balser and Wixon, 2009). The temperature dependence of decomposition can weaken the capacity of humid tropical forests to act as carbon sinks, intensifying feedbacks between climate and the global carbon cycle (Corlett, 2016). To anticipate these responses, it is essential to develop quantitative models that capture the temperature dependence of carbon mineralization processes (Nottingham et al., 2020; O'Connell et al., 2018). In humid tropical soils, temperature can influence SOC dynamics through multiple pathways, one of which is its effects on Fe^{III} reduction, which may enhance carbon mineralization (Barcellos et al., 2018a; Hall et al., 2013; Yao and Conrad, 2000). Understanding the temperature response of these Fe-C processes is therefore critical to accurately predict soil carbon fluxes and their feedback on microbial activity and mineral dynamics.

Numerous studies have examined the effects of warming on soil heterotrophic respiration (Dacal et al., 2022; Chari et al., 2021; Romero-Olivares et al., 2017; Allison et al., 2010; Carey et al., 2016; Melillo et al., 2017) as well as organic matter decomposition (Conant et al., 2011; Davidson et al., 2012; Allison et al., 2010; Oliverio et al., 2017). Collectively, these studies demonstrate that increasing temperature generally accelerates microbial respiration and organic matter decomposition, leading to enhanced CO_2 efflux and shifts in microbial community composition, depending on substrate availability, moisture, and microbial thermal adaptation. Yet, the temperature dependence of Fe redox dynamics in humid tropical soils remains comparatively understudied compared with other soil processes and ecosystems, with most evidence on Fe redox processes from temperate and wetland ecosystems. For instance, Schilling et al. (2019) reported that microbial Fe^{III} reduction in subalpine wetland soils exhibited strong temperature dependency (Q_{10} ranges 1.5–8.9). Pallud et al. (2020) similarly found broad temperature responses in wetland soils (Q_{10} = 0.8–5.3), while Curtinrich et al. (2022) found that warming enhanced Fe^{III} reduction and altered carbon-nutrient fluxes also in peatland soils. In addition, incubation experiments that integrate temperature and redox manipulations (Chari et al., 2021) revealed that elevated temperatures further intensified Fe^{III} reduction and CO_2 release under reducing conditions. Soil-warming experiments in humid tropical regions have focused primarily on bulk carbon and nutrient cycling (Giardina et al., 2014; Kimball et al., 2018; Nottingham et al., 2020; Balser and Wixon, 2009) and less on specific Fe-mediated pathways that regulate carbon mineralization and stabilization. This gap is critical because Fe oxides and Fe-reducing or Fe-oxidizing microbes can exert strong control over SOC dynamics, particularly in humid tropical soils where

https://doi.org/10.5194/egusphere-2026-2111
Preprint. Discussion started: 22 April 2026

fluctuating redox conditions can mediate both carbon release and protection (Calabrese et al., 2020; Barcellos et al., 2025; Lin et al., 2021).

Given the coupling between Fe redox, microbial, and DOC processes, the temperature response of an Fe process (e.g., Fe^{III} reduction) inferred from model fitting depends on what processes are explicitly included in the model. For example, a reduction rate coefficient estimated using a change in Fe^{II} between two time points (i.e., linear interpolation) would differ from one estimated based on multiple time points using Monod kinetics that includes the influence of Fe^{III} availability. While detailed consideration of all the processes controlling Fe redox dynamics may increase realism, the feasibility of using higher-order models depends on data availability. Avoiding overfitting requires carefully balancing model complexity with the limitations of empirical observations (Fang and Gentine, 2024; Cameron et al., 2022). Bayesian calibration provides a powerful framework for integrating biogeochemical theory with observational data while accounting for parameter and data uncertainties (Clifford et al., 2014). Specifically, Bayesian approaches enable full probabilistic characterization of model parameters through posterior distributions that integrate prior knowledge with likelihood functions, potentially providing robust predictions grounded in both theory and data (Xie et al., 2020). Bayesian inference, particularly when implemented through ensemble samplers in Markov Chain Monte Carlo (MCMC), can reveal complex, non-linear behaviors, parameter correlations, and multimodal distributions inherent in soil biogeochemical systems.

In addition to quantifying parameter uncertainty, model selection should be based on metrics that account for this uncertainty and penalize model complexity (e.g., more parameters). Unlike traditional goodness-of-fit metrics (e.g. the coefficient of determination R^2, which only quantifies the distance between mean prediction and observation), probabilistic model assessment metrics, including the Watanabe-Akaike Information Criterion (WAIC), Log Pseudo Marginal Likelihood (LPML), and Leave-One-Out Cross-Validation (LOO), enable evaluation of the trade-off between model fit and complexity. These metrics account for full posterior uncertainty and provide a more nuanced and probabilistically grounded assessment of model performance. Importantly, they penalize overfitting and unnecessary complexity (Gelman et al., 2014), ensuring that selected models are not only accurate in fitting observed data but also generalizable and robust in predictive contexts. While detailed consideration of all the processes controlling Fe redox dynamics may increase realism, the feasibility of using higher-order models depends on data availability.

Here, we sought to quantify the temperature dependence of Fe reduction under constant anoxic conditions in humid tropical soils and to enhance our mechanistic understanding of how temperature-driven Fe redox cycling influences soil carbon dynamics. To address this, we conducted controlled laboratory slurry incubations using soils collected from valley regions near the El Verde Field Station, Luquillo Experimental Forest, Puerto Rico. We monitored changes in Fe^{II} and Fe^{III} concentrations under anoxic conditions, where oxygen was maintained absent throughout the incubation at 23 °C, 27 °C, and 33 °C for 12 consecutive days. Slurry incubations were used to quantify potential Fe reduction rates under well-mixed conditions. Slurring in fact minimizes diffusion constraints, reduces microsite heterogeneity, and suppresses Fe^{II} re-oxidation relative to intact soils, enabling a clear assessment of intrinsic temperature controls on Fe^{III} reduction kinetics but with reduced relevance to structured and heterogeneous field soils. To capture Fe-reduction dynamics, we developed process-based models spanning four levels of mechanistic complexity. First, we introduced a one-pool Fe^{II} based model, in which Fe^{II} accumulation is treated as the sole dy-

https://doi.org/10.5194/egusphere-2026-2111
Preprint. Discussion started: 22 April 2026

namic state variable, while the reducible Fe^{III} pool is constrained using independently measured citrate–ascorbate extractable short-range-ordered (SRO) Fe. We then considered an alternative one-pool formulation based on 0.5 M HCl-extracted Fe^{III} kinetics derived from the slurry experiment. A two-pool model explicitly represented coupled Fe^{III} and Fe^{II} dynamics using slurry-derived measurements, and a three-pool model further incorporated dissolved organic carbon (DOC) to capture Fe–C interactions. Using a Bayesian inference approach, we estimated key temperature-dependent rate constants (r_{RED} and K_{RED}) and derived their corresponding Q_{10} and activation energy (Ea), providing quantitative insight into temperature dependence. Model performance was evaluated using the coefficient of determination (R^2) along with Bayesian model selection criteria, WAIC, LPML, and LOO, which enabled a rigorous comparison of model fit, complexity, and parameter uncertainty. This integrated modeling approach allowed us to estimate the temperature dependence of Fe reduction using the most suitable model structure with the lowest uncertainty.

2 Methodology

Soil samples were collected in June 2016 from the valley regions near the El Verde Field Station within the Luquillo Experimental Forest (LEF), Puerto Rico (Barcellos et al., 2018b). The sampling site is located in the Espíritu Santo watershed, part of the NSF-funded Luquillo Critical Zone Observatory (LCZO) and Long-Term Ecological Research (LTER) programs. This region receives a mean annual precipitation of approximately 3,500 mm y^{-1}, with low seasonality but occasionally experiences extreme rainfall events exceeding 100 mm d^{-1} due to Caribbean storm systems (Heartsill-Scalley et al., 2007). On average, there are about 225 rainy days per year (61.6 %), and the mean annual temperature is approximately 23 °C (Gross et al., 2018). Soils are predominantly classified as Inceptisols (Typic Eutrudepts) (Hall and Silver, 2015; Barcellos et al., 2018b) and the valleys are characterized by high soil moisture (prone to flooding) and a pH of approximately 6 (Barcellos et al., 2018b). Soil samples were collected from the surface to a depth of 15 cm and transported to the University of Georgia where they were sieved to 2 mm and air-dried until further use. In the lab, soil slurries were prepared with a 1:10 soil:solution ratio and incubated at 23 °C, 27 °C, and 33 °C. The incubation experiments were conducted in triplicate under anoxic conditions for 12 consecutive days to monitor temporal changes in 0.5 M HCl extractable Fe^{II} and Fe^{III} concentrations throughout the experiment. The 0.5 M HCl extraction effectively captures the pool of reactive Fe^{II} produced during microbial Fe^{III} reduction, whereas HCl-extractable Fe^{III} represents a labile but incomplete fraction of the total reducible Fe^{III} pool. To better constrain the total reducible iron reservoir, independently measured values of total reducible short-range-ordered Fe (SRO-Fe) for valley soils were incorporated, using published values from Barcellos et al. (2018b) and Ginn et al. (2017). These values were used to represent the size of the reducible Fe^{III} pool in model formulations where direct measurements were not available.

2.1 Modeling temperature dependency on Fe dynamics for constant anoxic conditions

To estimate the temperature dependence of Fe reduction dynamics under constant saturated (anoxic) conditions, we employed a series of models capturing different Fe-C interactions. We first consider a simple one pool model based on Fe^{II} accumulation, in which Fe^{II} is treated as the sole dynamic state variable. The size of the reducible Fe^{III} pool is constrained using indepen-

https://doi.org/10.5194/egusphere-2026-2111
Preprint. Discussion started: 22 April 2026

dently measured citrate–ascorbate extractable short-range-ordered (SRO) Fe from the El Verde field station (Ginn et al., 2017; Barcellos et al., 2018b), as this operationally defined fraction most closely represents the highly reactive, microbially reducible Fe^{III} phases available over the timescale of our anoxic incubations. While using SRO-Fe as an external constraint avoids relying on HCl-extractable Fe^{III} pools, which may not entirely represent the bioavailable reducible Fe fraction, we also implemented a complementary one pool model using 0.5 M HCl-extracted slurry time-series Fe^{III} observations to add dynamics to the available Fe^{III} pool. Model complexity was then progressively increased by introducing a two pool model that explicitly represents coupled Fe^{II} and Fe^{III} dynamics, leveraging measurements of both species to constrain Fe reduction processes. Finally, a three pool model was developed by incorporating a dissolved organic carbon (DOC) pool to account for potential Fe–C interactions. Although no observed DOC data were available, this formulation allows exploration of how carbon dynamics modulate the temporal evolution of Fe^{II} and Fe^{III}.

2.1.1 One pool Fe^{II} model

Under constant anoxic condition, a mass balance equation for Fe^{II} can be written as Ginn et al. (2017); Calabrese and Porporato (2019),

$$\frac{dFe^{II}}{dt} = RED, \tag{1}$$

where Fe^{II} represents the concentration of ferrous iron and RED is the microbial Fe^{III} reduction rate. Assuming mass conservation under closed conditions, the pool of reducible Fe^{III} is represented as $Fe^{Tot} - Fe^{II}$, where Fe^{Tot} denotes the citrate-ascorbate extractable SRO-Fe pool (although true total Fe is much higher). This operationally defined SRO-Fe fraction is considered to approximate the rapidly reducible Fe^{III} pool available to microorganisms (Barcellos et al., 2018b; Ginn et al., 2017). The reduction rate is expressed using the Michaelis-Menten type for formulation.

$$RED = r_{RED} \cdot \frac{Fe^{Tot} - Fe^{II}}{Fe^{Tot} - Fe^{II} + K_{\mathrm{RED}}}, \tag{2}$$

where r_{RED} is the maximum reduction rate and K_{RED} is the half saturation constant of the reduction reaction. This formulation accounts for enzymatic control and substrate limitation of microbial Fe^{III} reduction. This one pool model requires calibration of the two kinetic parameters (r_{RED} & K_{RED}) and total available Fe for reduction Fe^{Tot}.

2.1.2 One pool Fe^{III} model

While the previous model is developed to assimilate Fe^{II} data, we formulate an alternative one pool model to assimilate Fe^{III}. The mass balance equation for Fe^{III} under constant anoxic condition, can be written also from Ginn et al. (2017); Calabrese and Porporato (2019),

$$\frac{dFe^{III}}{dt} = -RED, \tag{3}$$

https://doi.org/10.5194/egusphere-2026-2111
Preprint. Discussion started: 22 April 2026

where Fe^{III} is the concentration of ferric iron and RED is the reduction rate, which in this case can be expressed directly as a function of Fe^{III}

$$RED = r_{RED} \cdot \frac{Fe^{III}}{Fe^{III} + K_{\mathrm{RED}}}, \tag{4}$$

where r_{RED} is the rate constant and K_{RED} is the half saturation constant of the reduction reaction. This one pool model also requires calibration of the two kinetic parameters (r_{RED} & K_{RED}) and the initial condition of Fe^{III} (t=0).

2.1.3 Two pool model (Fe^{II} and Fe^{III})

Since HCl extracted time-series data are available for both Fe^{II} and Fe^{III} from the slurry experiment, the two pool model explicitly represents both Fe pools. The balance equations for Fe^{II} and Fe^{III} under anoxic conditions can be written as

$$\frac{dFe^{II}}{dt} = RED \tag{5}$$

$$\frac{dFe^{III}}{dt} = -RED. \tag{6}$$

where RED is computed similarly following Eq. (4). The oxidation of Fe^{II} to Fe^{III} is not considered as we assume complete absence of O_2, in line with the experimental conditions. The two-pool model does not introduce any new kinetic parameters, but it does add the initial Fe^{II} condition as a parameter to be calibrated.

2.1.4 Three pool model (Fe^{II}, Fe^{III}, and DOC)

To investigate how additional processes affect model calibration and uncertainty, the three pool model further incorporates the dissolved organic carbon (DOC) pool, for which no data are available. This allows us to test whether the additional model flexibility translates into additional predictive power or uncertainty. Under the conditions of the soil slurries, the temporal change in DOC concentration is controlled by the microbial uptake of DOC, a process linked to the microbial reduction of Fe^{III} ($U_{\mathrm{DOC-Fe^{III}}}$)—among many other anaerobic processes—and the release of Fe-mineral-associated (sorbed or trapped) organic matter (FeOM) as DOC, denoted as F_{fd}

$$\frac{dDOC}{dt} = -U_{DOC-Fe^{III}} + F_{fd} \tag{7}$$

Under anoxic conditions, Fe-based DOC uptake can be estimated from the reduction reaction (RED) and the stoichiometric coefficient (β) representing the molar ratio of Fe reduced per mole of carbon decomposed

$$U_{DOC-Fe^{III}} = \frac{RED}{\beta} \tag{8}$$

With the inclusion of DOC, the reduction kinetics (RED) can also be expressed based on the availability of DOC as an additional limiting factor

$$RED = r_{RED} \cdot \frac{Fe^{III}}{Fe^{III} + K_{\mathrm{RED}}} \cdot \frac{DOC}{DOC + K_{\mathrm{DOC}}} \tag{9}$$

https://doi.org/10.5194/egusphere-2026-2111
Preprint. Discussion started: 22 April 2026

The release of DOC (F_{fd}) is influenced by the concentration of Fe mineral-associated organic carbon (FeOM) (Huang and Hall, 2017) and can be estimated as proportional to the change in Fe^{III} concentrations over time through a coefficient (q_{maxfe}) representing the concentration of DOC released per unit Fe^{III}. This process is described by

$$F_{fd} = q_{maxfe} \cdot \frac{dFe^{III}}{dt} \tag{10}$$

Combining these expressions, the overall DOC dynamics under constant anoxic conditions can be written as

$$\frac{dDOC}{dt} = -\frac{RED}{\beta} + q_{maxfe} \cdot \frac{dFe^{III}}{dt} \tag{11}$$

where the full coupling with the dynamics of Fe^{III} is more explicit. Because of the additional interactions, the three pool model adds K_{DOC}, q_{maxfe}, and the initial condition of DOC (t=0) to the list of parameters to be calibrated.

2.2 Bayesian calibration

The values of the kinetic parameters across the three experimental temperatures were obtained through Bayesian calibration. In particular, we used the *emcee* package (Foreman-Mackey et al., 2013) in Python, which employs the Affine Invariant Ensemble Sampler for Markov Chain Monte Carlo (MCMC). The ensemble sampler uses multiple walkers that explore the parameter space concurrently, improving efficiency and handling complex, correlated distributions. We used 64 walkers, each running for 5,000 iterations, resulting in a total of 320,000 samples. To allow for chain stabilization, the first 300 iterations of each walker were discarded as burn-in (300×64), leaving 300,800 samples for the posterior analysis. In MCMC calibration, the processing rate (iterations per second) decreases as additional parameters are introduced, since they increase model complexity and the dimensionality of the parameter space. Convergence and mixing (efficient exploration of the posterior) were assessed through visual inspection of trace plots. The retained samples were used to estimate posterior means, credible intervals, and to evaluate model performance. Lognormal informative priors (Table S2) were employed to initialize the runs, with the parameters of the prior distributions selected based on expert judgment and earlier empirical findings (Allison et al., 2010; Li et al., 2014; Barcellos et al., 2018b; Ginn et al., 2017; Huang and Hall, 2017). The likelihood function was formulated assuming the logarithm of normally distributed residuals between observed and model-predicted Fe^{III} concentrations in linear space, allowing for a direct and interpretable measure of model performance. This approach ensures parameter estimates span realistic ranges consistent with biogeochemical models. Overall, using *emcee* for Bayesian calibration allows for a more nuanced understanding of the soil C-Fe model, addressing both parameter uncertainty and model complexity, thus enhancing the reliability of predictions.

2.3 Information criteria and cross validation

Bayesian model evaluation relies on metrics that account for uncertainty in parameter estimates and predictive accuracy across the posterior distribution. Among the most widely recommended are the Widely Applicable Information Criterion (WAIC), Leave-One-Out Cross-Validation (LOO), and the Log Pseudo-Marginal Likelihood (LPML). These methods provide more robust measures of model fit compared to classical criteria like Akaike Information Criterion (AIC) and Bayesian Information

https://doi.org/10.5194/egusphere-2026-2111
Preprint. Discussion started: 22 April 2026

Criterion (BIC) which rely solely on point estimates and do not capture the full posterior uncertainty inherent in Bayesian models fitted via Markov Chain Monte Carlo (MCMC) (Xie et al., 2020). WAIC and LOO both estimate out-of-sample predictive performance using posterior samples, with lower values indicating better model performance (Vehtari et al., 2017). LPML, derived from the conditional predictive ordinate (CPO), aggregates predictive densities for each observation left out of the model (Chen et al., 2012); higher LPML values suggest superior predictive fit. In contrast, AIC and BIC are either non-Bayesian or only partially Bayesian, and they tend to perform poorly in non-linear models due to reliance on asymptotic assumptions or single point estimates (Spiegelhalter et al., 2002; Gelman et al., 2014; Vehtari et al., 2017). Therefore, WAIC, LOO, and LPML are preferred for model comparison. In addition to these Bayesian metrics, we also report the classical coefficient of determination (R^2), which provides a familiar and interpretable measure of variance explained by the model and remains a useful complement for comparing model predictions to observed data.

2.4 Estimation of temperature dependency

After running the MCMC simulation, the kinetic constants calibrated at the three temperatures are fitted to Q_{10} and Arrhenius models to estimate the Q_{10} and activation energy (Ea) values, which quantify the temperature dependence of biologically-mediated processes. This analysis is conducted across the four models, allowing us to investigate how model complexity for given data availability impacts the estimates of temperature dependence.

The Q_{10}, which quantifies the temperature dependency of a process, is calculated from the slope of the log-linear relationship between rates and temperature

$$r_2 = r_1 Q_{10}^{(\frac{T-T_0}{10})} \tag{12}$$

In this equation, r_2 represents the value of rate constants (r_{RED}, K_{RED}, K_{DOC}) at temperature T, while Q_{10} is the corresponding rate at the reference temperature T_0 (i.e., 23 °C). Each rate constant was analyzed separately to determine its temperature dependency. The activation energy (Ea) is estimated similarly, from the following equation

$$r = Ae^{-(\frac{E_a}{RT})} \tag{13}$$

Where r denotes the value of rate constants (r_{RED}, K_{RED}, K_{DOC}) at temperature T and A denotes a pre-exponential factor associated with the rate constants, and R is the universal gas constant.

We note that the MCMC calibration of the model equations (Eq. (4) and Eq. (9)) was used to estimate the kinetic parameters independently at each temperature, without incorporating the Q_{10} and Arrhenius formulations a priori. This way, the estimation of the parameters variation with temperature is not constrained by the specific temperature-dependence formulation. The Q_{10} and Arrhenius equations are later fitted to the calibrated parameters to estimate their temperature dependence metrics (Q_{10} and Ea). This also allows us to test the validity of both the Q_{10} and Arrhenius models for soil Fe reduction kinetics.

https://doi.org/10.5194/egusphere-2026-2111
Preprint. Discussion started: 22 April 2026

3 Results

This study aims to quantify the temperature dependence of Fe reduction under constant anoxic conditions in humid tropical soils and to advance the mechanistic understanding of how temperature-driven Fe redox cycling regulates soil carbon dynamics. To accomplish this, we present the calibration results, examining the temperature dependence of reduction dynamics using four models of increasing complexity. The performance of each model is then evaluated based on goodness of fit, model complexity, and uncertainty.

3.1 Overall *T* patterns

The calibrated kinetic parameters of the reduction kinetics for the four models at three different temperatures (23, 27, and 33 °C) are summarized in Table 1 (numbers in parentheses indicate the standard deviation of the estimates). The reaction rate r_{RED} increases with temperature across all models, consistent with the expected temperature dependence of reaction kinetics. The half saturation constant K_{RED} generally increases with temperature in the two and three pool models. In contrast, the value of K_{RED} remain almost same at the one pool Fe^{II} model with increasing temperature, while in the one pool Fe^{III} model, the value at 27 °C is slightly lower than at 23 °C. The coefficient (q_{maxfe}) in the three pool model remains unchanged across temperatures. While the initial concentration of Fe^{III} and Fe^{II} exhibit minor fluctuations with temperature across the models (as expected due to experimental uncertainty), the initial DOC concentration decreases with increasing temperature. The values of different initial conditions are provided in Table S1.

3.2 Fe reduction in the one pool Fe^{II} model

The one pool Fe^{II} model successfully reproduces the temporal increase in Fe^{II} concentrations under constant anoxic conditions at all three temperatures (23, 27, and 33 °C). At 23 °C, the modeled Fe^{II} concentration increases steadily over the 12-day period, closely matching the observed data with minimal deviations (Figure 1a). The trajectories exhibit an approximately linear increasing trend, indicating a nearly constant net reduction rate under these conditions. At 27 °C, Fe^{II} accumulation occurs more rapidly, consistent with enhanced microbial reduction at elevated temperature, and the modeled curve aligns well with observations, with minor discrepancies around day 5. At 33 °C, the model predicts the fastest Fe^{II} accumulation, and the observed data follow the same overall trend. Overall, the strong agreement across temperatures indicates that the one pool Fe^{II} model effectively captures the temperature dependence of Fe reduction dynamics, although the larger deviations at higher temperatures may suggest the increasing influence of additional processes not explicitly represented in this simplified formulation.

The posterior probability density functions (PDFs) of the reduction rate constant (r_{RED}) shift toward higher values with increasing temperature, see Figure 1b. Mean r_{RED} increases from approximately 6.4 mmol $kg^{-1}d^{-1}$ at 23 °C to about 9.6 mmol $kg^{-1}d^{-1}$ at 33 °C. The distribution at 23 °C is relatively narrow, suggesting strong parameter constraint, while the distribution at 27 °C is noticeably wider, indicating greater uncertainty or variability in the estimated rates at intermediate temperature. At 33 °C, the distribution is moderate in width, wider than at 23 °C but narrower than at 27 °C, suggesting improved constraint

https://doi.org/10.5194/egusphere-2026-2111
Preprint. Discussion started: 22 April 2026

Table 1. Calibrated kinetic parameters, including the reduction rate (r_{RED}), half-saturation constants (K_{RED} and K_{DOC}), and coefficient (q_{maxfe}), are shown for 23 °C, 27 °C, and 33 °C across all four models. Uncertainties are given in parentheses.

T (°C)	r_{RED} (mmol kg^{-1} d^{-1})	K_{RED} (mmol kg^{-1})	K_{DOC} (mmol kg^{-1})	q_{maxfe} (unitless)
One pool Fe^{II} model				
23	6.40 (±0.15)	8.03 (±0.99)	–	–
27	7.22 (±0.43)	8.03 (±1.01)	–	–
33	9.61 (±0.27)	8.00 (±0.99)	–	–
One pool Fe^{III} model				
23	9.19 (±0.36)	9.45 (±1.12)	–	–
27	10.13 (±0.35)	8.50 (±1.08)	–	–
33	15.97 (±0.66)	15.28 (±2.31)	–	–
Two pool model (Fe^{II} and Fe^{III})				
23	7.96 (±0.20)	7.36 (±0.81)	–	–
27	9.88 (±0.32)	8.34 (±1.07)	–	–
33	15.95 (±0.64)	15.74 (±2.26)	–	–
Three pool model (Fe^{II}, Fe^{III}, and DOC)				
23	9.09 (±0.33)	6.38 (±0.72)	3.77 (±0.95)	0.37 (±0.03)
27	12.70 (±0.81)	7.40 (±0.90)	5.49 (±1.40)	0.37 (±0.03)
33	19.15 (±1.22)	7.86 (±0.96)	8.10 (±1.90)	0.37 (±0.03)

relative to 27 °C while still reflecting increased variability at higher temperature. Despite temperature specific differences, the relatively narrow distributions indicate good parameter identifiability. In contrast to r_{RED}, the posterior distributions of the half-saturation constant (K_{RED}) largely overlap across temperatures. Mean values remain close to 8 mmol kg^{-1} (Figure 1c), indicating that temperature primarily influences the rate of reduction rather than its dependence on Fe availability.

The estimated r_{RED} values show a strong positive relationship with temperature, with both the Q_{10} and Arrhenius models providing excellent fits ($R^2 > 0.98$). The estimated Q_{10} value (1.50) and Arrhenius activation energy (30.65 kJ mol^{-1}) suggest moderate temperature dependency, but still consistent with biologically mediated redox reactions (Figure 1d). The half-saturation constant exhibits minimal variation with temperature, as reflected by the near-zero activation energy and Q_{10} ~ 1 (Figure 1e). This means microbes reduce Fe faster at higher temperatures, indicating that temperature mainly regulates microbial metabolic rates (r_{RED}), while their dependence on Fe availability stays roughly unchanged.

https://doi.org/10.5194/egusphere-2026-2111
Preprint. Discussion started: 22 April 2026

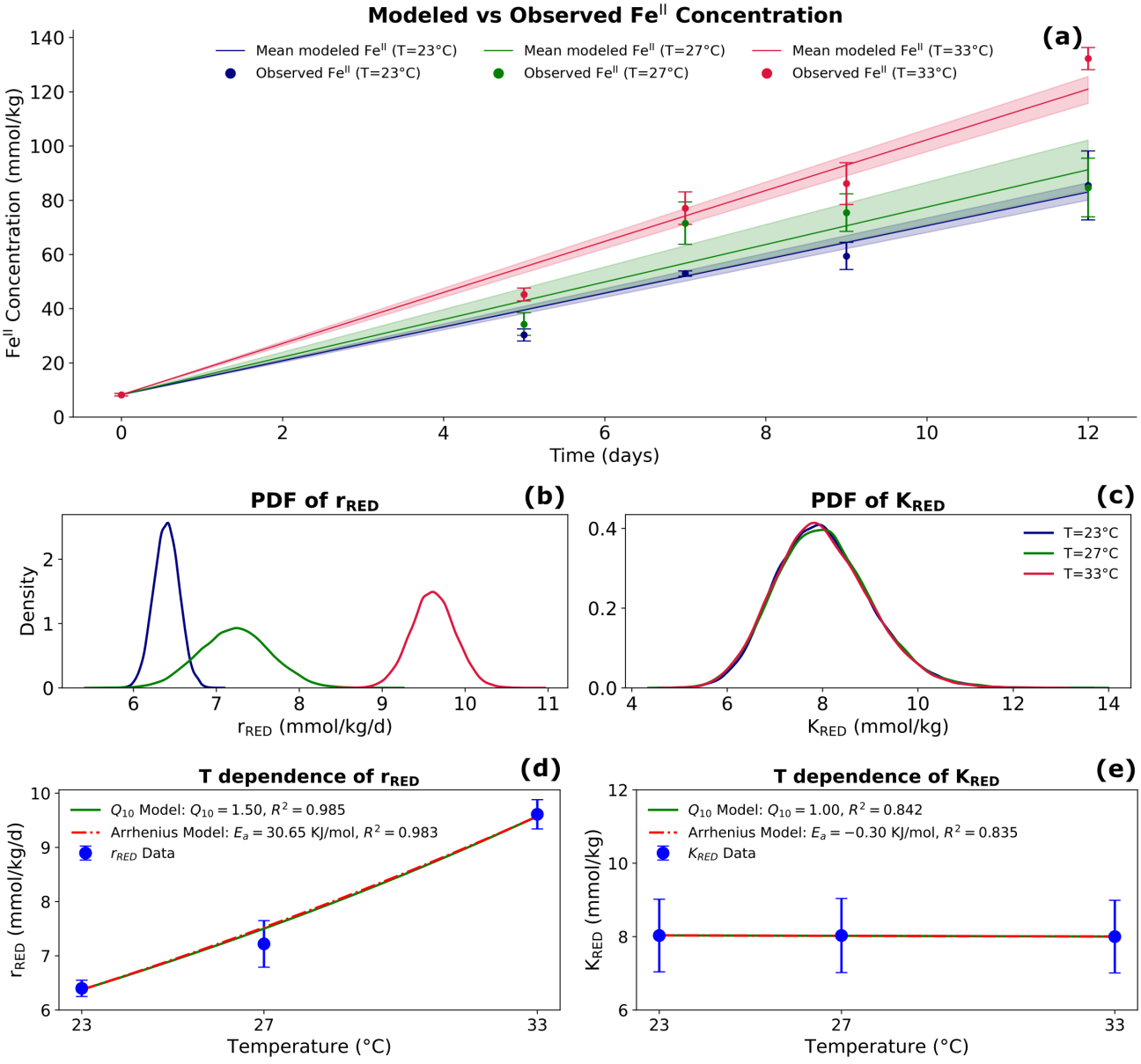

Figure 1. Temperature-dependent dynamics of the Fe^{II} pool and corresponding model fits. (a) Observed and modeled Fe^{II} concentration over time at 23 °C, 27 °C, and 33 °C. Solid line represents mean model predictions and shaded regions indicate 95% confidence intervals. Dots correspond to observed Fe^{II} concentrations at each temperature. Probability density functions (PDFs) of the estimated rate constants (b) r_{RED} and (c) K_{RED} for Fe^{II} accumulation at each temperature. Temperature dependence of (d) r_{RED} and (e) K_{RED}, fitted using the Q_{10} model (green line) and the Arrhenius model (red dashed line). Experimental data are shown with error bars. Model fitted parameters (Q_{10}, Ea) and coefficients of determination (R^2) are annotated within each plot.

https://doi.org/10.5194/egusphere-2026-2111
Preprint. Discussion started: 22 April 2026

3.3 Fe reduction through the one pool Fe^{III} model

At 23 °C, the modeled Fe^{III} concentration decreases steadily over the 12-day period, closely matching the observed data, as indicated by minimal deviations (Figure 2a). At 27 °C, the rate of Fe^{III} decline is slightly faster, reflecting the effect of elevated temperature on system dynamics. The modeled trajectory at this temperature also aligns well with the observed points, though moderate discrepancies are again noticeable at day 5. At 33 °C, the model predicts the most rapid decline in Fe^{III} concentration, but with more evident deviations particularly on days 7 and 9. Compared to the one pool Fe^{II} model, which showed nearly linear Fe^{II} accumulation and slightly tighter agreement with observations across temperatures, the Fe^{III} only formulation exhibits greater deviations at higher temperatures. This likely occurs because HCl-extractable Fe^{III} represents a mixed Fe pool that does not uniquely correspond to the reactive Fe^{III} phases available for microbial reduction (Hyacinthe et al., 2006) and therefore introduces more uncertainty in the representation of the reducible Fe pool (Slotznick et al., 2020). In contrast the one pool Fe^{II} model is better constrained by independently measured citrate–ascorbate SRO-Fe, which more directly represents the pool of highly reactive Fe minerals available for microbial reduction. Overall, the agreement between modeled and observed data across all three temperatures indicates that the model captures the temperature dependence of Fe^{III} dynamics, although with deviations at higher temperatures as also found for the one pool Fe^{II} model.

The posterior probability density function (PDFs) of r_{RED} again shifts clearly towards higher values as temperature increases (Figure 2b, c), reflecting a positive temperature dependency. In contrast, the PDFs of K_{RED} do not exhibit a clear trend. While the distribution at 33 °C shifts towards higher values, the distributions at 23 and 27 °C show significant overlap. This pattern indicates that the temperature dependence of the half saturation constant is more evident at higher temperatures. It should be emphasized that parameter uncertainty (i.e., spread of the distribution) is larger at 33 °C for both kinetic paramaters. In contrast, the one pool Fe^{II} model exhibited relatively stable K_{RED} values across temperatures with narrower distributions, suggesting better parameter identifiability when Fe^{II} accumulation is used to constrain kinetics.

For the reaction rate r_{RED}, the fitted value of Q_{10} is 1.77 (Figure 2d). The model provides a great fit to the data, with an R^2 value of 0.952. The Arrhenius model also demonstrates a good correlation, with an estimated activation energy for this process is 43.03 kJ mol^{-1}, with R^2 value of 0.948 (Figure 2d). Similarly, for K_{RED}, the fitted Q_{10} value was obtained as 1.58, indicating the lower temperature dependency compared to r_{RED} with lower R^2 value (0.705). The activation energy is lower (33.93 kJ mol^{-1}) with lower R^2 value (0.691) compared to r_{RED}. By contrast, the one pool Fe^{II} model indicated minimal temperature dependence and stronger consistency across temperatures. Overall, both Q_{10} and Arrhenius models are able capture the increasing trend of r_{RED} and K_{RED} with temperature (although r_{RED} shows slightly more dependence on temperature), reinforcing the temperature dependence of the reduction process.

3.4 Fe reduction through the two pool model (Fe^{II} and Fe^{III})

The results of the two pool model can be compared with the observed concentrations of both Fe^{II} and Fe^{III}, see Figure 3a. Overall, the dynamics of both species demonstrate a clear temperature dependence. The Fe^{III} dynamics follow a pattern similar to that seen in the one pool Fe^{III}model, with faster declines at higher temperatures, indicating enhanced reduction rates. How-

https://doi.org/10.5194/egusphere-2026-2111
Preprint. Discussion started: 22 April 2026

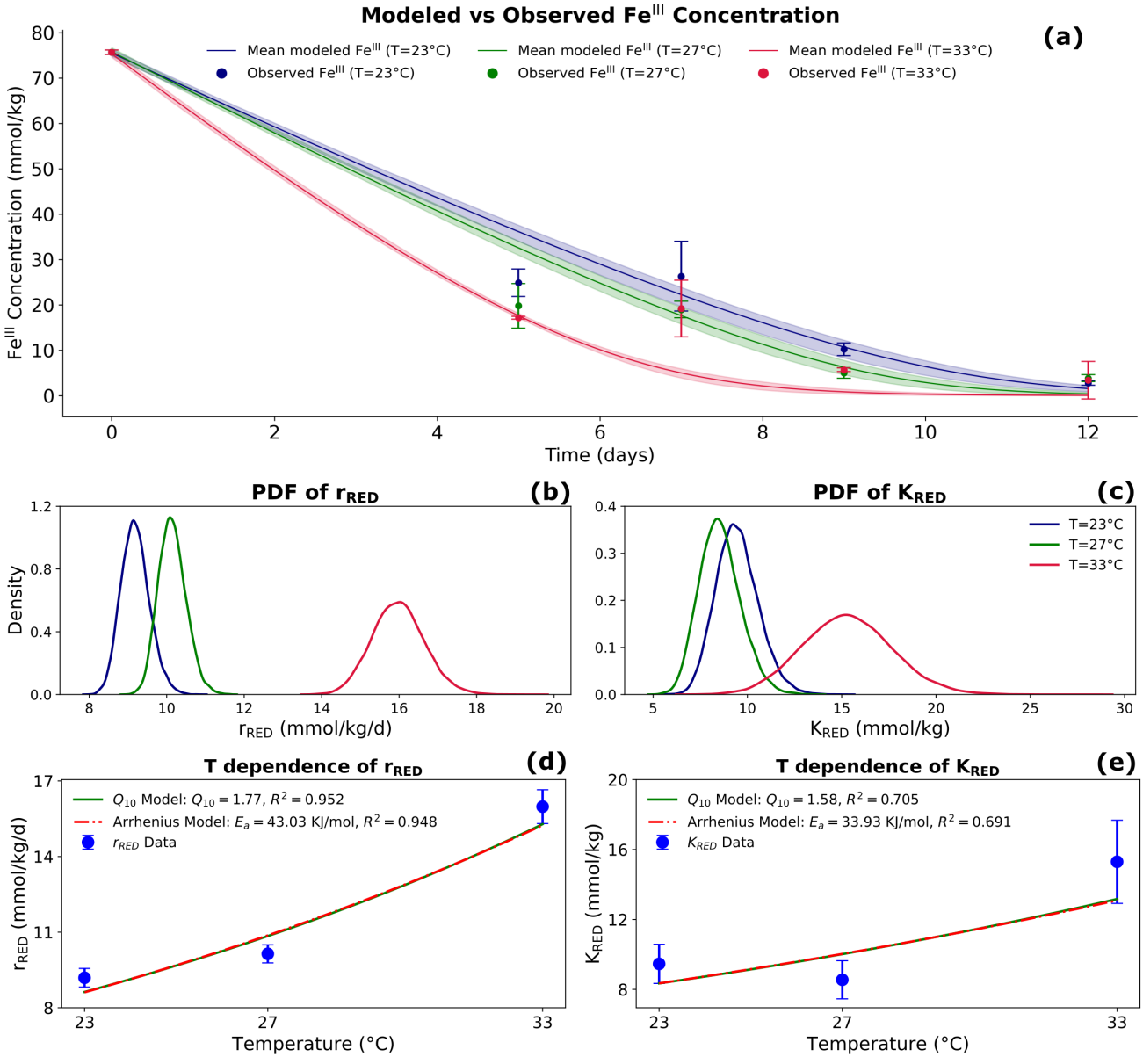

Figure 2. Temperature-dependent dynamics of the Fe^{III} pool and corresponding model fits. (a) Observed and modeled Fe^{III} concentration over time at 23 °C, 27 °C, and 33 °C. Solid line represents mean model predictions and shaded regions indicate 95% confidence intervals. Dots correspond to observed Fe^{III} concentrations at each temperature. Probability density functions (PDFs) of the estimated rate constants (b) r_{RED} and (c) K_{RED} for Fe^{III} reduction at each temperature. Temperature dependence of (d) r_{RED} and (e) K_{RED}, fitted using the Q_{10} model (green line) and the Arrhenius model (red dashed line). Experimental data are shown with error bars. Model parameters and coefficients of determination (R^2) are annotated within each plot.

https://doi.org/10.5194/egusphere-2026-2111
Preprint. Discussion started: 22 April 2026

ever, while the one pool Fe^{II} model shows nearly linear Fe^{II} accumulation, the HCl-extracted data show a non-linear increase in Fe^{II}. Because the system is closed, the modeled accumulation of Fe^{II} should generally track the reduction of Fe^{III}. However, a discrepancy is observed at day 12, where the decrease in Fe^{III} is not fully matched by a corresponding increase in Fe^{II}. In particular, the observed Fe^{II} concentration reaches 136 mmol/kg, whereas the model does not reproduce this value because no additional Fe^{III} reduction is predicted at that time. This mismatch further illustrates that HCl-extractable Fe^{III} only represents a portion of the pool of microbially reducible Fe^{III}.

The posterior probability density functions (PDFs) of the estimated rate constants (r_{RED} and K_{RED}) provide further insight into the temperature dependence of Fe^{III} reduction (Figure 3b,c). The non-overlapping PDFs of r_{RED} across temperatures indicate a strong temperature effect on the reduction rate relative to parameter uncertainty. Similar to the one pool models, the spread of the distributions increases with temperature, suggesting greater variability in Fe–C processes under warmer conditions. The PDFs of K_{RED} also show a clear temperature-dependent shifts, albeit with larger spread.

Temperature-dependence model fits are shown in Figure 3d,e. For r_{RED}, the Q_{10} model yielded a Q_{10} value of 1.97 with an R^2 value of 0.989 indicating a stronger temperature dependence. Similarly, the Arrhenius model estimated an activation energy (Ea) of 51.04 kJ mol^{-1}, higher than in the previous models. A similar pattern was observed for K_{RED}, which showed even stronger temperature dependence (Q_{10} = 2.11 and E_a = 55.90 kJ mol^{-1}). Overall, these results suggest that the two pool model leads to stronger temperature dependence in Fe reduction than estimated with the one pool models.

3.5 Fe reduction and DOC dynamics through the three pool model (Fe^{II}, Fe^{III} and DOC)

The three pool model extends the previous one pool Fe^{III} model and two pool models by incorporating an additional dissolved organic carbon (DOC) pool alongside the Fe^{II} and Fe^{III} pools. This enhancement allows for a more comprehensive representation of coupled redox dynamics and organic carbon transformations within the system, although DOC data are not available for this dataset.

The simulated Fe^{III} concentration gradually declines over time, accompanied by a steady increase in Fe^{II} similar to the two pool model. As Fe reduction proceeds, modeled DOC concentrations also decrease, implying that the release of mineral associated organic carbon (FeOM)— estimated as proportional to the change in Fe^{III} concentrations through the coefficient q_{maxfe}—does not keep up with the simultaneous microbial DOC uptake. Consistent with the one and two pool models, the temporal trends in Fe^{III} and Fe^{II} clearly reflect temperature dependent reaction kinetics, with the highest rates observed at 33 °C, followed by 27 °C and 23 °C. This highlights the strong influence of temperature on both redox transformations and carbon cycling.

Similar to the previous models, the PDFs of r_{RED} (Figure 4b) shift systematically toward higher values with increasing temperature. The clear separation between distributions indicates a strong temperature dependency of r_{RED}, but broader tails, especially at 27 °C and 33°C, suggest greater uncertainty in parameter estimates, likely due to the added complexity and higher number of unconstrained parameters (the model extends to DOC dynamics, but without DOC data). In contrast, while the PDFs of K_{RED} (Figure 4c) also shift rightward with temperature, the distributions show considerable overlap across temperatures. This overlap suggests that, although there is a trend of increasing K_{RED} with temperature, the uncertainty in K_{RED} can be confused

https://doi.org/10.5194/egusphere-2026-2111
Preprint. Discussion started: 22 April 2026

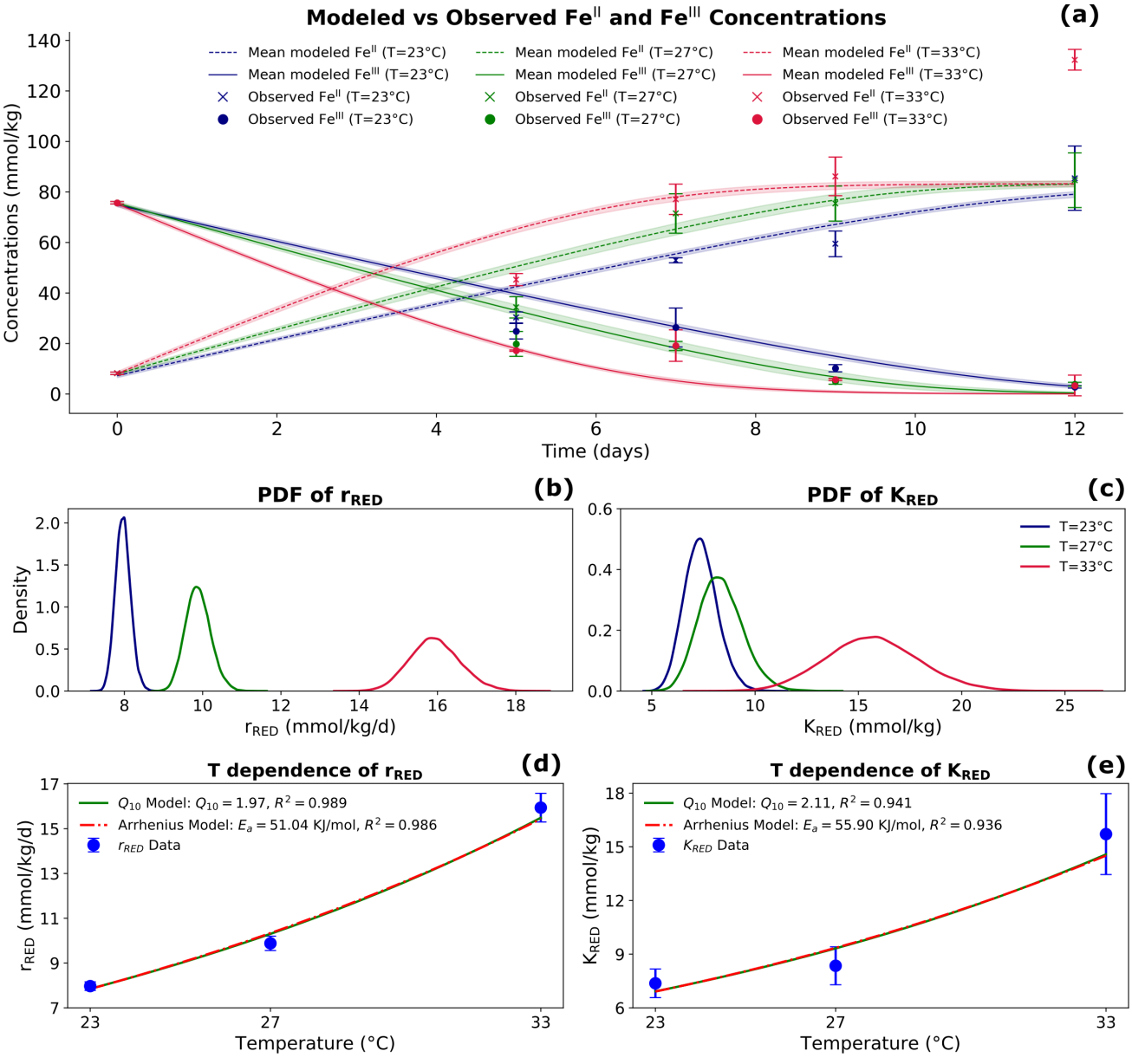

Figure 3. Temperature-dependent dynamics of the Fe^{II} and Fe^{III} pools and corresponding model fits. (a) Observed and modeled Fe^{II} and Fe^{III} concentrations over time at 23 °C, 27 °C, and 33 °C. Solid line represents mean model predictions and shaded regions indicate 95% confidence intervals. Dots correspond to observed Fe^{III} concentrations and the cross represents observed Fe^{II} concentrations for the temperatures. Probability density functions (PDFs) of the estimated rate constants (b) r_{RED} and (c) K_{RED} for Fe^{III} reduction at each temperature. Temperature dependence of (d) r_{RED} and (e) K_{RED}, fitted using the Q_{10} model (green line) and the Arrhenius model (red dashed line). Experimental data are shown with error bars. Model parameters and coefficients of determination (R^2) are annotated within each plot.

https://doi.org/10.5194/egusphere-2026-2111
Preprint. Discussion started: 22 April 2026

with the temperature dependence. Together, these patterns demonstrate that the three pool model can capture complex system behavior but with larger uncertainty than simpler one pool and two pool models. These considerations will be quantitatively analyzed using appropriate performance metrics below.

For r_{RED}, in line with the two pool model, the Q_{10} model yielded a value of 2.12 with an R^2 = 0.996 (Figure 4d), indicating strong temperature dependence, with a substantially better fit to the data compared to the one and two pool models. The Arrhenius model further supports this trend, estimating an activation energy (E_a) of 56.52 kJ mol^{-1} with an even higher R^2 = 0.998 (Figure 4e). For K_{RED}, a Q_{10} value of 1.23 and Ea = 15.46 kJ mol^{-1}, provided moderate fits relative to two pool model (R^2= 0.881 and R^2 = 0.887, respectively), and indicate lower temperature dependency in line with the one pool models.

3.6 Evaluation of model fit and predictive performance of four models at varying temperatures

WAIC, LPML, LOO and R^2 metrics were calculated to assess model performance and its variation across temperatures (23 °C, 27 °C, and 33 °C) for the one pool (Fe^{II} & Fe^{III}), two pool, and three pool models (Figure 5). Predictive performance varied with temperature across all models. The WAIC and LOO (with lower values indicating better predictive performance), generally indicated improved model performance at 27 °C compared to 23 °C for most model structures. For example, the two pool model showed a decrease in WAIC from 129.51 at 23 °C to 87.36 at 27 °C and a corresponding decrease in LOO from 106.76 to 79.33. A similar improvement was observed for the three pool model, where WAIC decreased from 161.51 to 85.40 and LOO decreased from 116.60 to 71.97 between 23 °C and 27 °C. Consistent with these trends, the LPML, where higher values indicate better predictive performance, increased (became less negative) for the two pool model from –67.68 to –45.09 and for the three pool model from –88.77 to –44.71 over the same temperature range. However, predictive performance deteriorated markedly at 33 °C, particularly for the more complex models. For instance, the two pool model exhibited a sharp increase in WAIC from 87.36 at 27 °C to 484.56 at 33 °C and in LOO from 79.33 to 354.07, while LPML declined from –45.09 to –230.28. Similar trends were observed for the three pool model. In contrast, the one pool models showed comparatively smaller changes across temperatures. Overall, our results indicate that model predictive performance is generally strongest at 27 °C and declines substantially at 33 °C, particularly for more complex model structures. These trends were mirrored in the R^2 values, where predictive accuracy declined substantially at 33 °C for the two and three pool models, dropping from 0.94 and 0.93 to 0.75 and 0.72, respectively, whereas it remained relatively high with R^2 of 0.93 for the one pool Fe^{III} model and 0.97 for one pool Fe^{II} model at 33 °C.

Overall, the Bayesian fit metrics consistently favored both the one pool models with higher fit for one pool Fe^{II} model across all temperatures. This likely reflects both its ability to fit the data as well as its lower effective complexity and uncertainty. The two and three pool models, on the contrary, showed good fit at lower temperatures only, with uncertainty increasing significantly at higher temperatures. These findings suggest that, while the more complex models may better capture dynamic redox behaviors under certain conditions, more data are necessary to constrain the additional parameters and leverage their potential without increasing uncertainty.

https://doi.org/10.5194/egusphere-2026-2111
Preprint. Discussion started: 22 April 2026

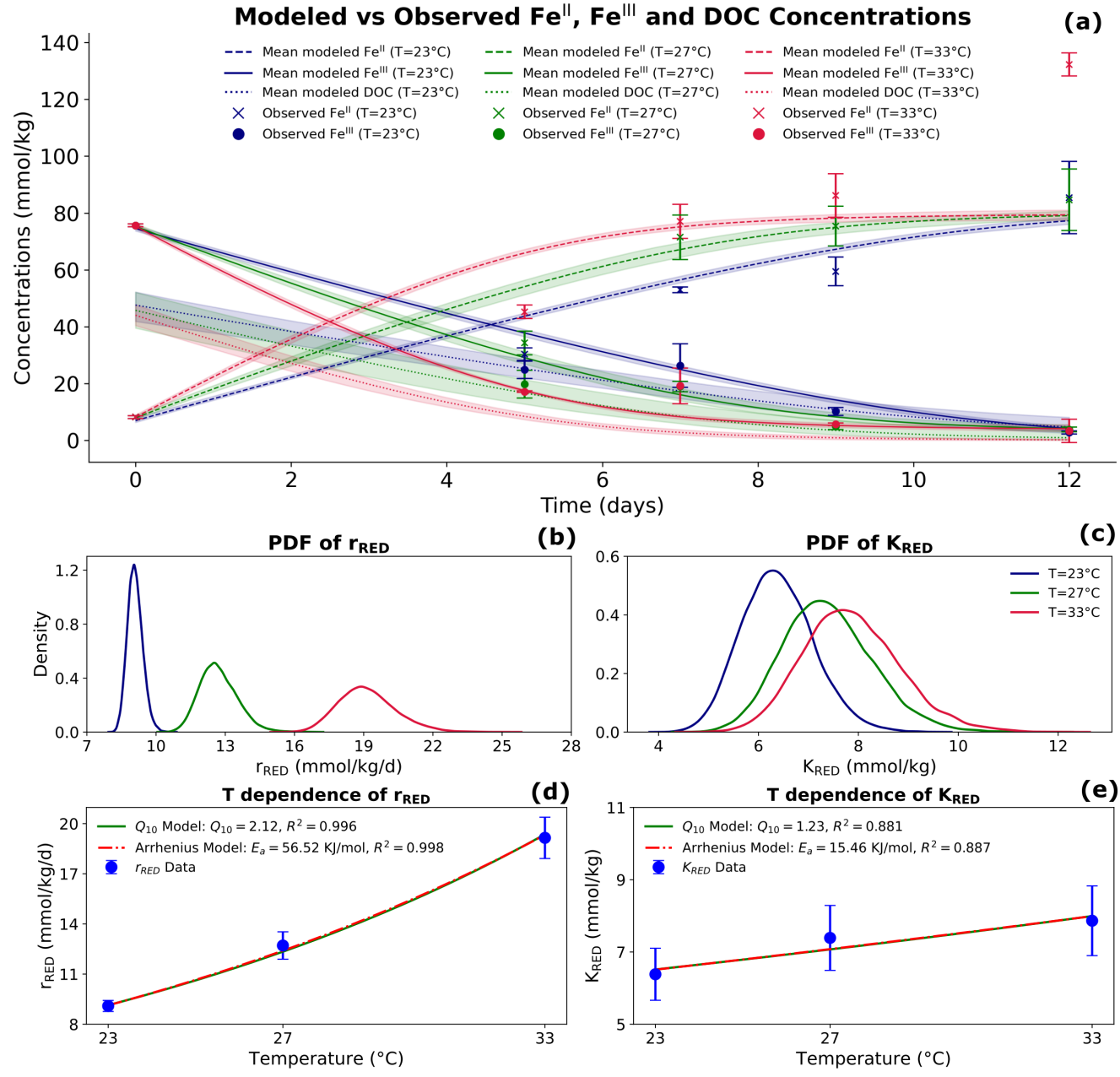

Figure 4. Temperature-dependent dynamics of the Fe^{II}, Fe^{III} and DOC pools and corresponding model fits. (a) Observed and modeled Fe^{II} and Fe^{III} concentrations and modeled DOC concentrations over time at 23 °C, 27 °C, and 33 °C. Solid line represents mean model predictions and shaded regions indicate 95% confidence intervals. Dots correspond to observed Fe^{III} concentrations and the cross represents observed Fe^{II} concentrations for the temperatures. Probability density functions (PDFs) of the estimated rate constants (b) r_{RED} and (c) K_{RED} for Fe^{III} reduction at each temperature. Temperature dependence of (d) r_{RED} and (e) K_{RED}, fitted using the Q_{10} model (green line) and the Arrhenius model (red dashed line). Experimental data are shown with error bars. Model parameters and coefficients of determination (R^2) are annotated within each plot.

https://doi.org/10.5194/egusphere-2026-2111
Preprint. Discussion started: 22 April 2026

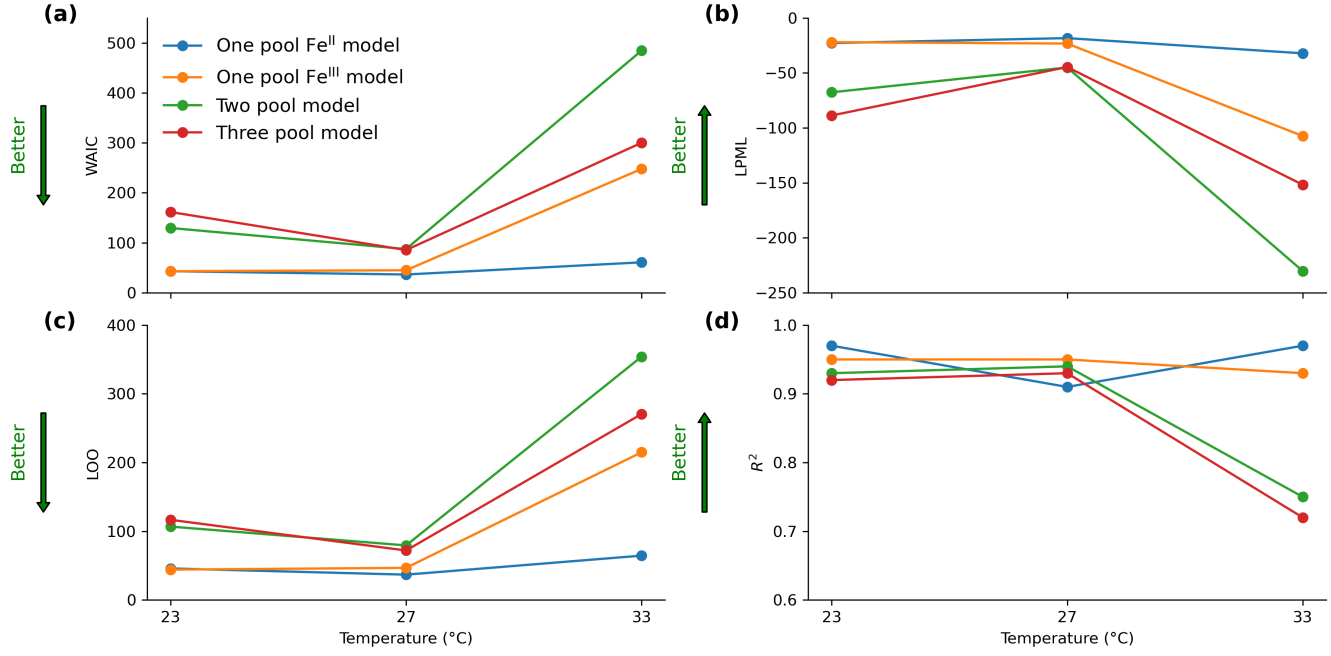

Figure 5. Comparison of model performance metrics across three temperatures (23°C, 27°C, and 33°C) for one, two, and three pool model. (a) WAIC, (b) LPML, (c) LOO, and (d) combined (Fe^{II} and Fe^{III}) coefficient of determination (R^2) values. Green arrows on the y-axis indicate the direction of improved performance.

4 Discussion and Implications

4.1 Temperature dependence of Fe reduction

In Fe-rich humid tropical soils, such as the those in the Luquillo Experimental Forest (Bhattacharyya et al., 2022; Barcellos et al., 2018b; Gross et al., 2018), warming may influence SOC decomposition through several pathways, one of which is temperature-dependent Fe reduction. By combining experimental data with models of Fe reduction, our analysis confirms the strong dependence of Fe^{III} reduction dynamics on temperature during anoxic conditions. The experimental results clearly highlight the impact of temperature on the temporal evolution of Fe^{III} and Fe^{II}, with faster reduction at higher temperature. Reduction rate coefficients ranged from about 6 mmol $kg^{-1}d^{-1}$ at 23 °C to about 19 mmol $kg^{-1}d^{-1}$ at 33 °C, broadly in line with rates observed in previous slurry experiments with similar valley soils (1.68 to 23.28 mmol $kg^{-1}d^{-1}$) (Ginn et al., 2017; Barcellos et al., 2018a; Tishchenko et al., 2015; Calabrese et al., 2020).

The temperature dependence of Fe reduction kinetics varied depending on the selected model, increasing, for example, from Q_{10} = 1.51 (and Ea = 30.83 kJ mol^{-1}) for the one pool Fe^{II} model to Q_{10} = 2.12 (and Ea = 56.51 kJ mol^{-1}) for the three pool model. The observed Q_{10} values for Fe reduction (1.51–2.12) fall within the range commonly reported for other microbial processes (1.5–2.5) under mesophilic temperature ranges (10–40 °C) (Davidson and Janssens, 2006; Conant et al., 2011). Our

https://doi.org/10.5194/egusphere-2026-2111
Preprint. Discussion started: 22 April 2026

estimates are also within the range of microbial growth Q_{10} values observed across latitudes, ranging from 1.15–1.73 in Arctic, 0.89–2.47 in Boreal, 0.92–2.01 in Temperate, and 1.14–2.55 in Tropical regions (Wang et al., 2021; Balser and Wixon, 2009), where geographic patterns in Q_{10} may arise not only from abiotic environmental differences, but also from shifts in dominant microbial taxa (Wang et al., 2021). Comparable temperature dependencies have also been observed for other anaerobic redox pathways—including nitrate, sulfate, and Fe^{III} reduction—where microbial activity and electron-transfer kinetics are closely linked to thermodynamic constraints (Jin and Bethke, 2007; Bethke et al., 2011).

Although these comparisons indicate that Fe-reducing microorganisms respond to temperature in ways consistent with other enzymatic soil processes, fully evaluating their impact on microbial respiration and SOC turnover necessitates quantifying CO_2 fluxes and distinguishing contributions from aerobic versus anaerobic pathways in field conditions where they may be competing for substrate (Lovley, 1991; Nealson and Saffarini, 1994; Kuzyakov, 2006). Moreover, since Fe can promote SOC decomposition under anoxic conditions yet facilitate SOC stabilization under oxic conditions, predicting the net effect of warming on SOC dynamics demands accounting for concurrent shifts in soil moisture regimes that regulate the alternation between oxic and anoxic states (Sierra et al., 2015; Bhattacharyya et al., 2018).

4.2 Balancing model complexity and uncertainty in Fe redox modeling using Bayesian calibration

Our analysis demonstrated how the temperature dependency is also a property of the selected model—not only of the specific biogeochemical reaction being considered. The appropriate model depends on the specific application and can be selected based on performance metrics that consider uncertainty and complexity to balance process representation with data availability (Feng, 2020). Structural choices can in fact affect apparent system sensitivity, as shown by Bonan et al. (2019), suggesting that some of the observed temperature dependency may result from model structure, not solely from underlying reaction kinetics. In this regard, the Bayesian framework provided a transparent, flexible, and uncertainty-aware approach for calibrating competing model structures and evaluating their performance, partially addressing equifinality and parameter non-identifiability challenges common in biogeochemical modeling (Tang et al., 2024; Tang and Zhuang, 2008; Marschmann et al., 2019).

Posterior distributions of key kinetic parameters (e.g., r_{RED}, K_{RED}) revealed how different models capture system behavior and the degree to which each parameter is constrained within our short-term anoxic incubations. This is evident from the emergent Fe reduction kinetics, illustrated in Figure 6 (horizontal and vertical dashed lines indicate r_{RED} and K_{RED}, respectively, at each temperature). Interestingly, the kinetics are more clustered for the one pool Fe^{II} model, where a significant increase in the reduction rate is observed only at 33 °C (lower Q_{10}). As the model complexity increases, Fe reduction rates become more distinct as temperature varies from 23 °C to 33 °C (higher Q_{10}), although with considerably larger uncertainty, as evident from the confidence bands, and confirmed by the performance metrics (Figure 5).

Among our four selected models, our performance metrics consistently pointed to the one pool Fe^{II} model as the most reliable (good fitting, lower parameter uncertainty) for capturing Fe reduction dynamics across the three temperatures. By contrast, the three pool model improved the representation of redox dynamics, but parameter uncertainty remained high. This result is highly dependent on the selected candidate models as well as the available data. A higher temporal resolution dataset or a more complete dataset in terms of quantities being measured could favor a more complex model. These observations

https://doi.org/10.5194/egusphere-2026-2111
Preprint. Discussion started: 22 April 2026

align with broader insights from carbon-cycle modeling, where the balance between model complexity and data constraints is a key consideration (Famiglietti et al., 2021). Increased structural detail improves predictions only when parameters are well informed by data (Famiglietti et al., 2021), while excessive complexity can increase uncertainty (Malmborg et al., 2024). These insights are particularly valuable for modeling redox processes in humid tropical soils, where historical data are often sparse and environmental conditions fluctuate rapidly. Incorporating additional observations (such as DOC concentrations or CO_2 fluxes) into future Bayesian calibration efforts could further enhance the predictive power and generalization of mechanistic redox models across diverse ecosystems, especially to confidently predict all the Fe-SOC interactions modulating SOC stabilization and mineralization.

4.3 Limitations and future research

Our model-data integration allowed us to estimate the temperature dependence of Fe reduction under constant anoxic conditions for a 'short' 12-day incubation period. However, short-term observations may not reflect long-term dynamics. Over extended timescales, microbial communities can adapt to sustained warming (Oechel et al., 2000; Min et al., 2019), which might potentially alter their metabolic efficiency and Fe redox behavior. Shifts in microbial composition and the temperature dependency of heterotrophic respiration have been widely studied in different regions (Romero-Olivares et al., 2017; Carey et al., 2016; Luo et al., 2001), but research in humid tropical regions remains limited in terms of Fe-reducing microorganisms. Investigation of changes microbial community compositions, in particular Fe reducers, and emergent traits in soils exposed to long-term warming (for example, from long-term warming experiments, such as SWELTR, Panama (Nottingham et al., 2020) and TRACE, Puerto Rico (Kimball et al., 2018; Wood et al., 2025)) may shed light into changes in temperature dependence over time.

Well-structured forest soils often exhibit substantial biogeochemical heterogeneity, with diverse microsite conditions coexisting within the soil matrix (Parkin, 1987; Hall and Silver, 2013). Incubating soil slurries, as done in our study, disrupts this structure and homogenizes biogeochemical conditions (Kuzyakov, 2006; Hall and Silver, 2013), thereby removing a source of variability that would be difficult to control experimentally or represent in models. Under these homogenized conditions, reactions proceed in an idealized, well-mixed environment, enabling us to estimate potential reaction rates. Assessing actual *in situ* rates, however, would require an experimental design that can preserve a degree of soil heterogeneity while still ensuring repeatability and reproducibility, as demonstrated in previous studies examining redox-driven processes, including microbial community responses (Pett-Ridge and Firestone, 2005), nitrogen cycling dynamics (Pett-Ridge et al., 2006), CO_2 respiration from litter and soil organic matter (Lin et al., 2021), and iron-mediated DOC stabilization and release (Bhattacharyya et al., 2018).

5 Conclusions

Using a Bayesian model-data integration, we estimated the temperature dependence of Fe reduction rates under anoxic and biogeochemically homogeneous (slurry) soil conditions for humid tropical soils from Luquillo Experimental Forest, Puerto

https://doi.org/10.5194/egusphere-2026-2111
Preprint. Discussion started: 22 April 2026

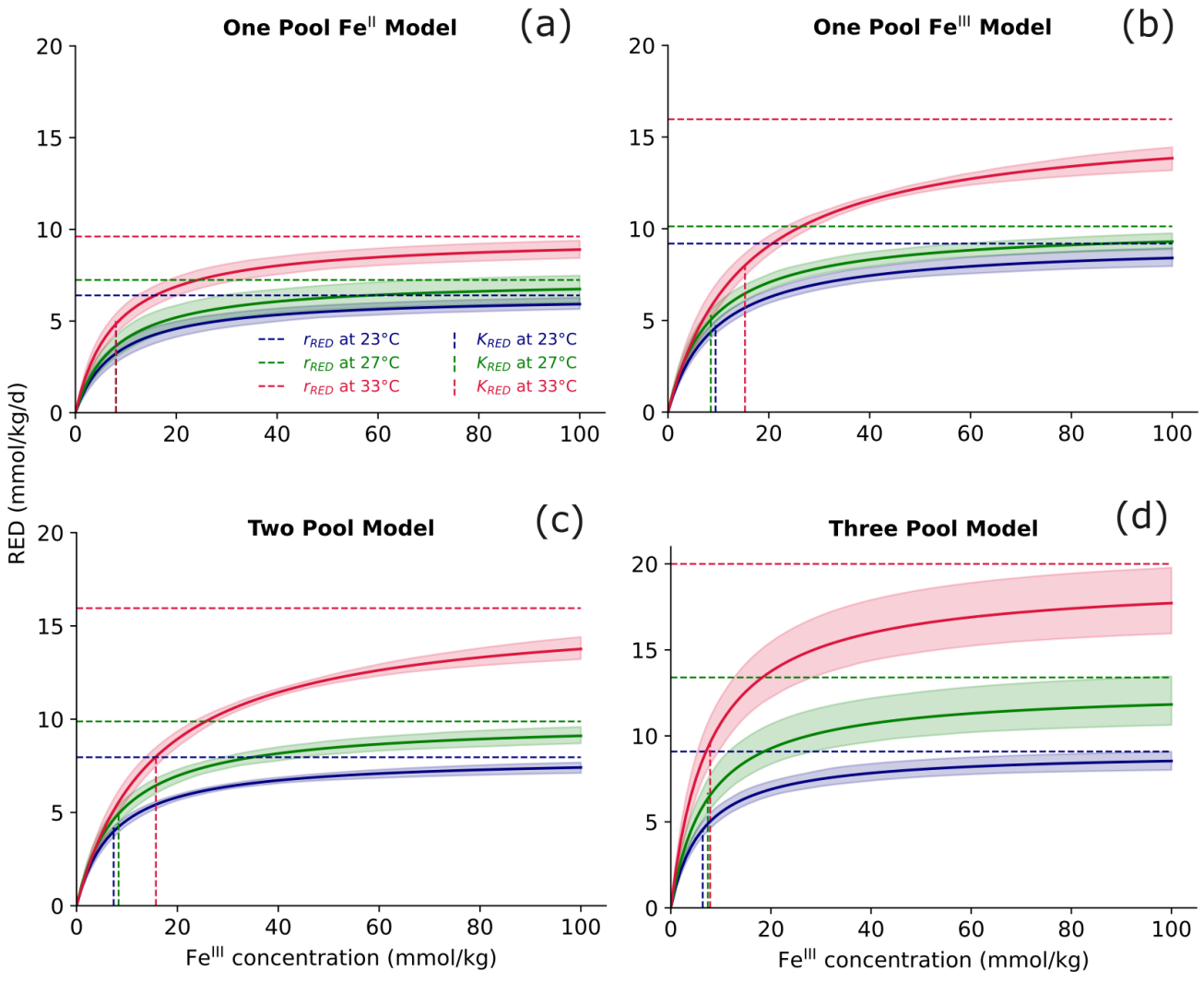

Figure 6. Relationship between Fe^{III} concentration and modeled Fe^{III} reduction rate (RED) for the one, two, and three pool models across three temperatures (23, 27, 33 °C). Solid lines represent mean RED curves generated from posterior parameter samples, with shaded regions indicating 95% confidence intervals. Dashed horizontal lines represent the maximum rate constants (r_{RED}) for each temperature, while dashed vertical lines mark the corresponding half-saturation constants (K_{RED}). Panels (a-d) illustrate the increasing separation among temperature responses and broader dynamic range in RED with increasing model complexity.

https://doi.org/10.5194/egusphere-2026-2111
Preprint. Discussion started: 22 April 2026

Rico. Across three different incubation temperatures, Fe reduction rates were clearly temperature dependent with microbial metabolic process Q_{10} values near 1.5 and Ea of $\sim$ 31 kJ mol^{-1}. Since estimates of temperature dependence varied with model structure, our analysis emphasized the importance of uncertainty in selecting the appropriate model. Bayesian metrics favored the simplest, one pool Fe^{II} model for the data available from our experiments. Importantly, our soil slurry approach minimized diffusion constraints and microsite heterogeneity, allowing isolation of intrinsic kinetic controls on Fe reduction. However, this approach may overestimate microbial access to resources and suppress the diversity of process rates that are supported by soil structural heterogeneity. Overall, These results provide a robust baseline for understanding temperature regulation of Fe redox processes and establish a foundation for extending analyses to more heterogeneous soil systems where physical constraints, such as diffusion limitations, along with spatially heterogeneous distribution of oxygen, substrates and microbial functionality, may modulate apparent temperature responses.

Code and data availability. The Python scripts used for MCMC calibration and figure generation, along with the original HCl-extracted Fe^{II} and Fe^{III} datasets, are available at: https://doi.org/10.5281/zenodo.19499750

Author contributions. SST developed the model, performed data analysis, and wrote the manuscript. SPC and AT conducted the laboratory experiments and contributed to manuscript revision. JPR contributed to experimental design and manuscript revision. SC contributed to model validation, supervision, and manuscript revision. SC, AT, and JPR contributed to funding acquisition.

Competing interests. The authors declare that there is no conflict of interest.

Acknowledgements. This research was supported by the U.S. National Science Foundation under Awards DEB-2241389, DEB-2241390 (to S.C., A.T. and J.P.R.). Work at Lawrence Livermore National Laboratory was conducted under the auspices of the U.S. DOE under Contract DE-AC52-07NA27344 with additional support provided by Award SCW1478. Portions of this research were conducted with the advanced computing resources provided by Texas A&M High Performance Research Computing. Any opinions, findings, and conclusions or recommendations expressed in this material are those of the author(s) alone.

https://doi.org/10.5194/egusphere-2026-2111
Preprint. Discussion started: 22 April 2026

References

Allison, S. D., Wallenstein, M. D., and Bradford, M. A.: Soil-carbon response to warming dependent on microbial physiology, Nature Geoscience, 3, 336–340, https://doi.org/10.1038/ngeo846, 2010.

Balser, T. C. and Wixon, D. L.: Investigating biological control over soil carbon temperature sensitivity, Global Change Biology, 15, 2935–2949, https://doi.org/10.1111/j.1365-2486.2009.01946.x, 2009.

Barcellos, D., Cyle, K. T., and Thompson, A.: Faster redox fluctuations can lead to higher iron reduction rates in humid forest soils, Biogeochemistry, 137, 367–378, https://doi.org/10.1007/s10533-018-0427-0, 2018a.

Barcellos, D., O'Connell, C. S., Silver, W., Meile, C., and Thompson, A.: Hot Spots and Hot Moments of Soil Moisture Explain Fluctuations in Iron and Carbon Cycling in a Humid Tropical Forest Soil, Soil Systems, 2, 59, https://doi.org/10.3390/soilsystems2040059, 2018b.

Barcellos, D., Pérez Castro, S., Campbell, A., Kimbrel, J. A., Blazewicz, S. J., Wollard, J., Pett-Ridge, J., and Thompson, A.: Duration of O2 Exposure Determines Dominance of FeII vs CH4 Production in Tropical Forest Soils, Environmental Science and Technology, 59, 4469–4481, https://doi.org/10.1021/acs.est.4c12329, 2025.

Bethke, C. M., Sanford, R. A., Kirk, M. F., Jin, Q., and Flynn, T. M.: The thermodynamic ladder in geomicrobiology, American Journal of Science, 311, 183–210, https://doi.org/10.2475/03.2011.01, 2011.

Bhattacharyya, A., Campbell, A. N., Tfaily, M. M., Lin, Y., Kukkadapu, R. K., Silver, W. L., Nico, P. S., and Pett-Ridge, J.: Redox Fluctuations Control the Coupled Cycling of Iron and Carbon in Tropical Forest Soils, Environmental Science and Technology, 52, 14 129–14 139, https://doi.org/10.1021/acs.est.8b03408, 2018.

Bhattacharyya, A., Kukkadapu, R. K., Bowden, M., Pett-Ridge, J., and Nico, P. S.: Fast redox switches lead to rapid transformation of goethite in humid tropical soils: A Mössbauer spectroscopy study, Soil Science Society of America Journal, 86, 264–274, https://doi.org/10.1002/saj2.20382, 2022.

Bonan, G. B., Lombardozzi, D. L., Wieder, W. R., Oleson, K. W., Lawrence, D. M., Hoffman, F. M., and Collier, N.: Model Structure and Climate Data Uncertainty in Historical Simulations of the Terrestrial Carbon Cycle (1850–2014), Global Biogeochemical Cycles, 33, 1310–1326, https://doi.org/10.1029/2019GB006175, 2019.

Calabrese, S. and Porporato, A.: Impact of ecohydrological fluctuations on iron-redox cycling, Soil Biology and Biochemistry, 133, 188–195, https://doi.org/10.1016/j.soilbio.2019.03.013, 2019.

Calabrese, S., Barcellos, D., Thompson, A., and Porporato, A.: Theoretical Constraints on Fe Reduction Rates in Upland Soils as a Function of Hydroclimatic Conditions, Journal of Geophysical Research: Biogeosciences, 125, 1–18, https://doi.org/10.1029/2020JG005894, 2020.

Cameron, D., Hartig, F., Minnuno, F., Oberpriller, J., Reineking, B., Van Oijen, M., and Dietze, M.: Issues in calibrating models with multiple unbalanced constraints: the significance of systematic model and data errors, Methods in Ecology and Evolution, 13, 2757–2770, https://doi.org/10.1111/2041-210X.14002, 2022.

Carey, J. C., Tang, J., Templer, P. H., Kroeger, K. D., Crowther, T. W., Burton, A. J., Dukes, J. S., Emmett, B., Frey, S. D., Heskel, M. A., Jiang, L., Machmuller, M. B., Mohan, J., Panetta, A. M., Reich, P. B., Reinsch, S., Wang, X., Allison, S. D., Bamminger, C., Bridgham, S., Collins, S. L., de Dato, G., Eddy, W. C., Enquist, B. J., Estiarte, M., Harte, J., Henderson, A., Johnson, B. R., Larsen, K. S., Luo, Y., Marhan, S., Melillo, J. M., Peñuelas, J., Pfeifer-Meister, L., Poll, C., Rastetter, E., Reinmann, A. B., Reynolds, L. L., Schmidt, I. K., Shaver, G. R., Strong, A. L., Suseela, V., and Tietema, A.: Temperature response of soil respiration largely unaltered with experimental warming, Proceedings of the National Academy of Sciences, 113, 13 797–13 802, https://doi.org/10.1073/pnas.1605365113, 2016.

https://doi.org/10.5194/egusphere-2026-2111
Preprint. Discussion started: 22 April 2026

Chari, N. R., Lin, Y., Lin, Y. S., and Silver, W. L.: Interactive effects of temperature and redox on soil carbon and iron cycling, Soil Biology and Biochemistry, 157, 108 235, https://doi.org/10.1016/j.soilbio.2021.108235, 2021.

Chen, M.-H., Shao, Q.-M., and Ibrahim, J. G.: Monte Carlo methods in Bayesian computation, Springer Science & Business Media, ISBN 1461212766, 2012.

Clifford, D., Pagendam, D., Baldock, J., Cressie, N., Farquharson, R., Farrell, M., Macdonald, L., and Murray, L.: Rethinking soil carbon modelling: A stochastic approach to quantify uncertainties, Environmetrics, 25, 265–278, https://doi.org/10.1002/env.2271, 2014.

Conant, R. T., Ryan, M. G., Ågren, G. I., Birge, H. E., Davidson, E. A., Eliasson, P. E., Evans, S. E., Frey, S. D., Giardina, C. P., Hopkins, F. M., Hyvönen, R., Kirschbaum, M. U., Lavallee, J. M., Leifeld, J., Parton, W. J., Megan Steinweg, J., Wallenstein, M. D., Martin Wetterstedt, J. , and Bradford, M. A.: Temperature and soil organic matter decomposition rates - synthesis of current knowledge and a way forward, Global Change Biology, 17, 3392–3404, https://doi.org/10.1111/j.1365-2486.2011.02496.x, 2011.

Corlett, R. T.: The Impacts of Droughts in Tropical Forests, Trends in Plant Science, 21, 584–593, https://doi.org/10.1016/j.tplants.2016.02.003, 2016.

Curtinrich, H. J., Sebestyen, S. D., Griffiths, N. A., and Hall, S. J.: Warming Stimulates Iron-Mediated Carbon and Nutrient Cycling in Mineral-Poor Peatlands, Ecosystems, 25, 44–60, https://doi.org/10.1007/s10021-021-00639-3, 2022.

Cusack, D. F., Karpman, J., Ashdown, D., Cao, Q., Ciochina, M., Halterman, S., Lydon, S., and Neupane, A.: Global change effects on humid tropical forests: Evidence for biogeochemical and biodiversity shifts at an ecosystem scale, Reviews of Geophysics, 54, 523–610, https://doi.org/10.1002/2015RG000510, 2016.

Dacal, M., Delgado-Baquerizo, M., Barquero, J., Berhe, A. A., Gallardo, A., Maestre, F. T., and García-Palacios, P.: Temperature Increases Soil Respiration Across Ecosystem Types and Soil Development, But Soil Properties Determine the Magnitude of This Effect, Ecosystems, 25, 184–198, https://doi.org/10.1007/s10021-021-00648-2, 2022.

Davidson, E. A. and Janssens, I. A.: Temperature sensitivity of soil carbon decomposition and feedbacks to climate change, Nature, 440, 165–173, https://doi.org/10.1038/nature04514, 2006.

Davidson, E. A., Samanta, S., Caramori, S. S., and Savage, K.: The Dual Arrhenius and Michaelis-Menten kinetics model for decomposition of soil organic matter at hourly to seasonal time scales, Global Change Biology, 18, 371–384, https://doi.org/10.1111/j.1365-2486.2011.02546.x, 2012.

Dubinsky, E. A., Silver, W. L., and Firestone, M. K.: Tropical forest soil microbial communities couple iron and carbon biogeochemistry, Ecology, 91, 2604–2612, https://doi.org/10.1890/09-1365.1, 2010.

Famiglietti, C. A., Smallman, T. L., Levine, P. A., Flack-Prain, S., Quetin, G. R., Meyer, V., Parazoo, N. C., Stettz, S. G., Yang, Y., Bonal, D., Bloom, A. A., Williams, M., and Konings, A. G.: Optimal model complexity for terrestrial carbon cycle prediction, Biogeosciences, 18, 2727–2754, https://doi.org/10.5194/bg-18-2727-2021, 2021.

Fang, J. and Gentine, P.: Exploring Optimal Complexity for Water Stress Representation in Terrestrial Carbon Models: A Hybrid-Machine Learning Model Approach, Journal of Advances in Modeling Earth Systems, 16, https://doi.org/10.1029/2024MS004308, 2024.

Feeley, K. J. and Silman, M. R.: Biotic attrition from tropical forests correcting for truncated temperature niches, Global Change Biology, 16, 1830–1836, https://doi.org/10.1111/j.1365-2486.2009.02085.x, 2010.

Feng, X.: Marching in step: The importance of matching model complexity to data availability in terrestrial biosphere models, Global Change Biology, 26, 3190–3192, https://doi.org/10.1111/gcb.15090, 2020.

Foreman-Mackey, D., Hogg, D. W., Lang, D., and Goodman, J.: emcee : The MCMC Hammer, Publications of the Astronomical Society of the Pacific, 125, 306–312, https://doi.org/10.1086/670067, 2013.

https://doi.org/10.5194/egusphere-2026-2111
Preprint. Discussion started: 22 April 2026

Gelman, A., Hwang, J., and Vehtari, A.: Understanding predictive information criteria for Bayesian models, Statistics and Computing, 24, 997–1016, https://doi.org/10.1007/s11222-013-9416-2, 2014.

Giardina, C. P., Litton, C. M., Crow, S. E., and Asner, G. P.: Warming-related increases in soil CO2 efflux are explained by increased below-ground carbon flux, Nature Climate Change, 4, 822–827, https://doi.org/10.1038/nclimate2322, 2014.

Ginn, B., Meile, C., Wilmoth, J., Tang, Y., and Thompson, A.: Rapid Iron Reduction Rates Are Stimulated by High-Amplitude Redox Fluctuations in a Tropical Forest Soil, Environmental Science and Technology, 51, 3250–3259, https://doi.org/10.1021/acs.est.6b05709, 2017.

Gross, A., Pett-Ridge, J., and Silver, W. L.: Soil Oxygen Limits Microbial Phosphorus Utilization in Humid Tropical Forest Soils, Soil Systems, 2, 65, https://doi.org/10.3390/soilsystems2040065, 2018.

Hall, S. J. and Silver, W. L.: Iron oxidation stimulates organic matter decomposition in humid tropical forest soils, Global Change Biology, 19, 2804–2813, https://doi.org/10.1111/gcb.12229, 2013.

Hall, S. J. and Silver, W. L.: Reducing conditions, reactive metals, and their interactions can explain spatial patterns of surface soil carbon in a humid tropical forest, Biogeochemistry, 125, 149–165, https://doi.org/10.1007/s10533-015-0120-5, 2015.

Hall, S. J., McDowell, W. H., and Silver, W. L.: When Wet Gets Wetter: Decoupling of Moisture, Redox Biogeochemistry, and Greenhouse Gas Fluxes in a Humid Tropical Forest Soil, Ecosystems, 16, 576–589, https://doi.org/10.1007/s10021-012-9631-2, 2013.

Heartsill-Scalley, T., Scatena, F., Estrada, C., McDowell, W., and Lugo, A.: Disturbance and long-term patterns of rainfall and throughfall nutrient fluxes in a subtropical wet forest in Puerto Rico, Journal of Hydrology, 333, 472–485, https://doi.org/10.1016/j.jhydrol.2006.09.019, 2007.

Huang, W. and Hall, S. J.: Elevated moisture stimulates carbon loss from mineral soils by releasing protected organic matter, Nature Communications, 8, https://doi.org/10.1038/s41467-017-01998-z, 2017.

Hyacinthe, C., Bonneville, S., and Van Cappellen, P.: Reactive iron(III) in sediments: Chemical versus microbial extractions, Geochimica et Cosmochimica Acta, 70, 4166–4180, https://doi.org/10.1016/j.gca.2006.05.018, 2006.

Jin, Q. and Bethke, C. M.: The thermodynamics and kinetics of microbial metabolism, American Journal of Science, 307, 643–677, https://doi.org/10.2475/04.2007.01, 2007.

Kimball, B. A., Alonso-Rodríguez, A. M., Cavaleri, M. A., Reed, S. C., González, G., and Wood, T. E.: Infrared heater system for warming tropical forest understory plants and soils, Ecology and Evolution, 8, 1932–1944, https://doi.org/10.1002/ece3.3780, 2018.

Kuzyakov, Y.: Sources of CO2 efflux from soil and review of partitioning methods, Soil biology and biochemistry, 38, 425–448, 2006.

Li, J., Wang, G., Allison, S. D., Mayes, M. A., and Luo, Y.: Soil carbon sensitivity to temperature and carbon use efficiency compared across microbial-ecosystem models of varying complexity, Biogeochemistry, 119, 67–84, https://doi.org/10.1007/s10533-013-9948-8, 2014.

Lin, Y., Campbell, A. N., Bhattacharyya, A., DiDonato, N., Thompson, A. M., Tfaily, M. M., Nico, P. S., Silver, W. L., and Pett-Ridge, J.: Differential effects of redox conditions on the decomposition of litter and soil organic matter, Biogeochemistry, 154, 1–15, https://doi.org/10.1007/s10533-021-00790-y, 2021.

Liptzin, D., Silver, W. L., and Detto, M.: Temporal Dynamics in Soil Oxygen and Greenhouse Gases in Two Humid Tropical Forests, Ecosystems, 14, 171–182, https://doi.org/10.1007/s10021-010-9402-x, 2011.

Lovley, D. R.: Dissimilatory Fe(III) and Mn(IV) reduction, Microbiological Reviews, 55, 259–287, https://doi.org/10.1128/mr.55.2.259-287.1991, 1991.

Luo, Y., Wan, S., Hui, D., and Wallace, L. L.: Acclimatization of soil respiration to warming in a tall grass prairie, Nature, 413, 622–625, https://doi.org/10.1038/35098065, 2001.

https://doi.org/10.5194/egusphere-2026-2111
Preprint. Discussion started: 22 April 2026

Malmborg, C. A., Willson, A. M., Bradley, L. M., Beatty, M. A., Klinges, D. H., Koren, G., Lewis, A. S. L., Oshinubi, K., and Woelmer, W. M.: Defining model complexity: An ecological perspective, Meteorological Applications, 31, 1–16, https://doi.org/10.1002/met.2202, 2024.

Marschmann, G. L., Pagel, H., Kügler, P., and Streck, T.: Equifinality, sloppiness, and emergent structures of mechanistic soil biogeochemical models, Environmental Modelling & Software, 122, 104 518, https://doi.org/10.1016/j.envsoft.2019.104518, 2019.

Melillo, J. M., Frey, S. D., DeAngelis, K. M., Werner, W. J., Bernard, M. J., Bowles, F. P., Pold, G., Knorr, M. A., and Grandy, A. S.: Long-term pattern and magnitude of soil carbon feedback to the climate system in a warming world, Science, 358, 101–105, https://doi.org/10.1126/science.aan2874, 2017.

Min, K., Buckeridge, K., Ziegler, S. E., Edwards, K. A., Bagchi, S., and Billings, S. A.: Temperature sensitivity of biomass-specific microbial exo-enzyme activities and CO 2 efflux is resistant to change across short- and long-term timescales, Global Change Biology, 25, 1793–1807, https://doi.org/10.1111/gcb.14605, 2019.

Nealson, K. H. and Saffarini, D.: Iron and manganese in anaerobic respiration: environmental significance, physiology, and regulation., Annual review of microbiology, 48, 311–344, 1994.

Nottingham, A. T., Meir, P., Velasquez, E., and Turner, B. L.: Soil carbon loss by experimental warming in a tropical forest, Nature, 584, 234–237, https://doi.org/10.1038/s41586-020-2566-4, 2020.

O'Connell, C. S., Ruan, L., and Silver, W. L.: Drought drives rapid shifts in tropical rainforest soil biogeochemistry and greenhouse gas emissions, Nature Communications, 9, https://doi.org/10.1038/s41467-018-03352-3, 2018.

Oechel, W. C., Vourlitis, G., Hastings, S., Zulueta, R., Hinzman, L., and Kane, D.: Acclimation of ecosystem CO2 exchange in the Alaskan Arctic, Nature, 406, 978–981, http://dx.doi.org/10.1038/35023137%5Cnhttp://www.nature.com/nature/journal/v406/n6799/suppinfo/406978a0_S1.html, 2000.

Oliverio, A. M., Bradford, M. A., and Fierer, N.: Identifying the microbial taxa that consistently respond to soil warming across time and space, Global Change Biology, 23, 2117–2129, https://doi.org/10.1111/gcb.13557, 2017.

Pallud, C., Rhoades, C. C., Schneider, L., Dwivedi, P., and Borch, T.: Temperature-induced iron (III) reduction results in decreased dissolved organic carbon export in subalpine wetland soils, Colorado, USA, Geochimica et Cosmochimica Acta, 280, 148–160, https://doi.org/10.1016/j.gca.2020.03.023, 2020.

Parkin, T. B.: Soil Microsites as a Source of Denitrification Variability, Soil Science Society of America Journal, 51, 1194–1199, https://doi.org/10.2136/sssaj1987.03615995005100050019x, 1987.

Pett-Ridge, J. and Firestone, M. K.: Redox Fluctuation Structures Microbial Communities in a Wet Tropical Soil, Applied and Environmental Microbiology, 71, 6998–7007, https://doi.org/10.1128/AEM.71.11.6998-7007.2005, 2005.

Pett-Ridge, J., Silver, W. L., and Firestone, M. K.: Redox Fluctuations Frame Microbial Community Impacts on N-cycling Rates in a Humid Tropical Forest Soil, Biogeochemistry, 81, 95–110, https://doi.org/10.1007/s10533-006-9032-8, 2006.

Roden, E. E.: Analysis of long-term bacterial vs. chemical Fe(III) oxide reduction kinetics, Geochimica et Cosmochimica Acta, 68, 3205–3216, https://doi.org/10.1016/j.gca.2004.03.028, 2004.

Roden, E. E. and Wetzel, R. G.: Organic carbon oxidation and suppression of methane production by microbial Fe(III) oxide reduction in vegetated and unvegetated freshwater wetland sediments, Limnology and Oceanography, 41, 1733–1748, https://doi.org/10.4319/lo.1996.41.8.1733, 1996.

Romero-Olivares, A., Allison, S., and Treseder, K.: Soil microbes and their response to experimental warming over time: A meta-analysis of field studies, Soil Biology and Biochemistry, 107, 32–40, https://doi.org/10.1016/j.soilbio.2016.12.026, 2017.

https://doi.org/10.5194/egusphere-2026-2111
Preprint. Discussion started: 22 April 2026

Scharlemann, J. P., Tanner, E. V., Hiederer, R., and Kapos, V.: Global soil carbon: Understanding and managing the largest terrestrial carbon pool, Carbon Management, 5, 81–91, https://doi.org/10.4155/cmt.13.77, 2014.

Schilling, K., Borch, T., Rhoades, C. C., and Pallud, C. E.: Temperature sensitivity of microbial Fe(III) reduction kinetics in subalpine wetland soils, Biogeochemistry, 142, 19–35, https://doi.org/10.1007/s10533-018-0520-4, 2019.

Sierra, C. A., Trumbore, S. E., Davidson, E. A., Vicca, S., and Janssens, I.: Sensitivity of decomposition rates of soil organic matter with respect to simultaneous changes in temperature and moisture, Journal of Advances in Modeling Earth Systems, 7, 335–356, https://doi.org/10.1002/2014MS000358, 2015.

Silva, L. C. R., Doane, T. A., Corrêa, R. S., Valverde, V., Pereira, E. I. P., and Horwath, W. R.: Iron-mediated stabilization of soil carbon amplifies the benefits of ecological restoration in degraded lands, Ecological Applications, 25, 1226–1234, https://doi.org/10.1890/14-2151.1, 2015.

Silva Neto, L. d. F. d., Inda, A. V., Bayer, C., Dick, D. P., and Tonin, A. T.: Óxidos de ferro em latossolos tropicais e subtropicais brasileiros em plantio direto, Revista Brasileira de Ciência do Solo, 32, 1873–1881, https://doi.org/10.1590/S0100-06832008000500008, 2008.

Slotznick, S. P., Sperling, E. A., Tosca, N. J., Miller, A. J., Clayton, K. E., van Helmond, N. A. G. M., Slomp, C. P., and Swanson-Hysell, N. L.: Unraveling the Mineralogical Complexity of Sediment Iron Speciation Using Sequential Extractions, Geochemistry, Geophysics, Geosystems, 21, https://doi.org/10.1029/2019GC008666, 2020.

Song, X., Wang, P., Van Zwieten, L., Bolan, N., Wang, H., Li, X., Cheng, K., Yang, Y., Wang, M., Liu, T., and Li, F.: Towards a better understanding of the role of Fe cycling in soil for carbon stabilization and degradation, Carbon Research, 1, 5, https://doi.org/10.1007/s44246-022-00008-2, 2022.

Souza, I. F., Almeida, L. F. J., Jesus, G. L., Pett-Ridge, J., Nico, P. S., Kleber, M., and Silva, I. R.: Carbon Sink Strength of Subsurface Horizons in Brazilian Oxisols, Soil Science Society of America Journal, 82, 76–86, https://doi.org/10.2136/sssaj2017.05.0143, 2018.

Spiegelhalter, D. J., Best, N. G., Carlin, B. P., and Van Der Linde, A.: Bayesian Measures of Model Complexity and Fit, Journal of the Royal Statistical Society Series B: Statistical Methodology, 64, 583–639, https://doi.org/10.1111/1467-9868.00353, 2002.

Tang, J. and Zhuang, Q.: Equifinality in parameterization of process-based biogeochemistry models: A significant uncertainty source to the estimation of regional carbon dynamics, Journal of Geophysical Research: Biogeosciences, 113, https://doi.org/10.1029/2008JG000757, 2008.

Tang, J., Riley, W. J., Manzoni, S., and Maggi, F.: Feasibility of Formulating Ecosystem Biogeochemical Models From Established Physical Rules, Journal of Geophysical Research: Biogeosciences, 129, https://doi.org/10.1029/2023JG007674, 2024.

Tang, Q., Li, W., Wang, J., Zhang, F., Dai, W., Li, Z., Wang, S., Yin, W., Cheng, Y., and Wang, X.: Coupled iron oxides and microbial-mediated soil organic carbon stabilization across tea plantation chronosequences, Soil and Tillage Research, 247, 106 382, https://doi.org/10.1016/j.still.2024.106382, 2025.

Thaymuang, W., Kheoruenromne, I., Suddhipraharn, A., and Sparks, D. L.: The Role of Mineralogy in Organic Matter Stabilization in Tropical Soils, Soil Science, 178, 308–315, https://doi.org/10.1097/SS.0b013e3182a4dac4, 2013.

Tishchenko, V., Meile, C., Scherer, M. M., Pasakarnis, T. S., and Thompson, A.: Fe2+ catalyzed iron atom exchange and re-crystallization in a tropical soil, Geochimica et Cosmochimica Acta, 148, 191–202, https://doi.org/10.1016/j.gca.2014.09.018, 2015.

Vehtari, A., Gelman, A., and Gabry, J.: Practical Bayesian model evaluation using leave-one-out cross-validation and WAIC, Statistics and Computing, 27, 1413–1432, https://doi.org/10.1007/s11222-016-9696-4, 2017.

Wang, C., Morrissey, E. M., Mau, R. L., Hayer, M., Piñeiro, J., Mack, M. C., Marks, J. C., Bell, S. L., Miller, S. N., Schwartz, E., Dijkstra, P., Koch, B. J., Stone, B. W., Purcell, A. M., Blazewicz, S. J., Hofmockel, K. S., Pett-Ridge, J., and Hungate, B. A.: The temperature sensitivity

https://doi.org/10.5194/egusphere-2026-2111
Preprint. Discussion started: 22 April 2026

of soil: microbial biodiversity, growth, and carbon mineralization, The ISME Journal, 15, 2738–2747, https://doi.org/10.1038/s41396-021-00959-1, 2021.

Wieder, W. R., Bonan, G. B., and Allison, S. D.: Global soil carbon projections are improved by modelling microbial processes, Nature Climate Change, 3, 909–912, https://doi.org/10.1038/nclimate1951, 2013.

Wood, T. E., Tucker, C., Alonso-Rodríguez, A. M., Loza, M. I., Grullón-Penkova, I. F., Cavaleri, M. A., O'Connell, C. S., and Reed, S. C.: Warming induces unexpectedly high soil respiration in a wet tropical forest, Nature Communications, 16, https://doi.org/10.1038/s41467-025-62065-6, 2025.

Xie, H. W., Romero-Olivares, A. L., Guindani, M., and Allison, S. D.: A Bayesian approach to evaluation of soil biogeochemical models, Biogeosciences, 17, 4043–4057, https://doi.org/10.5194/bg-17-4043-2020, 2020.

Yao, H. and Conrad, R.: Effect of temperature on reduction of iron and production of carbon dioxide and methane in anoxic wetland rice soils, Biology and Fertility of Soils, 32, 135–141, https://doi.org/10.1007/s003740000227, 2000.